Broadband antireflection property of silicon nanocone arrays with porous sidewalls fabricated by Ag-catalyzed etching

Fan Bai,[1,2] Yan Zhang,[1] Zhiqiang Duan,[1] Robert Hoye,[3] Mwenya Trevor,[1] Yingfeng Li,[1] and Meicheng Li[1,a]

[1]*State Key Laboratory of Alternate Electrical Power System with Renewable Energy Sources, North China Electric Power University, Beijing 102206, China*

[2]*National Quality Supervision & Inspection Center for Non-ferrous Metals (Yunnan), Kunming 650223, China*

[3]*Department of Materials Science & Metallurgy, University of Cambridge, CB2 3QZ, UK*

(Received 15 June 2017; accepted 24 August 2017; published online 11 September 2017)

Siliconnanocone (SiNC) arrays with porous sidewallswere successfully fabricated through a simple, low-cost Ag-catalyzed etching method. By electron spin resonance technique and TEM analysis, it has been verified that the formation of porous SiNC arrays is due to the gradual dissolution of the pristine Ag nanoislands as they sank into the Si and the lateral etching of the regenerated Ag nanoparticles to the SiNC sidewalls. Theoretical calculation results suggest that the reflectance of the porous SiNC arrays is much lower than that of the smooth SiNC arrays over wide wavelengths ranging from 300nm to 1700nm. The long-wavelength reflectance can be further suppressed by increasing surface porosity of the SiNCs and their length. Experimental test results show the lowest average reflectance of 1.7% in the wavelength range of 300-1000nm while approximately 30% in the wavelength ranges of 1200-1700nm, which is generally consistent with the theoretical results. This shows that the porous SiNC arrays had excellent broadband antireflection properties, making them attractive for a wide range of potential applications in Si-based optoelectronic devices. [http://dx.doi.org/10.1063/1.4990456]

INTRODUCTION

Surface antireflection techniques are important for improving the performance of many optoelectronic devices such as light emitting diodes, light sensors and solar cells.[1–4] In recent years, Si nanowire (SiNW) arrays have developed to be one of the most promising antireflection materials.[5–10] Usually, the SiNW arrays can suppress reflection in the wavelength range of 300-1000 nm but they are relatively poor in the wavelength range of 1200-1700 nm.[11,12] Hence, the development of SiNW arrays with broadband antireflection properties is necessary.

To achieve the goal of broadband antireflection, an effective approach is structural optimization of SiNW arrays. Tapering SiNW can further suppress surface reflection because of its profile of gradient reduction of effective refractive index from air to silicon.[13–15] Moreover, introducing a porous layer[16] or doping in other atoms[17] on nanowire sidewalls can enhance the absorption near the band edge of silicon, which is beneficial for reducing long-wavelength reflectance. Combining with the above structural advantages, we find that a composite structure of porous silicon naoncone (SiNC) arrays is an effective approach to achieve the goal of broadband antireflection.

Metal-assisted chemical etching is a simple fabrication method for producing porous SiNC arrays. A Au mesh is a catalyst for the production of such arrays.[18–21] At the Au/Si contacts, the excess holes

[a]To whom correspondence should be addressed. E-mail: mcli@ncepu.edu.cn

can diffuse along the nanocones from their root to tip, making the nanocone tips porous.[15,16] However, since Au is expensive this process is not ideal.

Ag is another catalyst for metal-assisted etching. We have reported the fabrication of SiNC arrays by using an Ag-catalyzed etching technique.[22] Recently we used silver nitrate solution as a catalyst to synthesize wafer-scale SiNC arrays with good surface quality.[23,24] However, the SiNC arrays with porous sidewalls prepared by Ag-assisted etching haven't been reported. The corresponding mechanism of the porous sidewalls formation in the Ag-catalyzed etching process is also unclear. In this work, the mechanism of the porous SiNC formation is systematically investigated based on the redox reactions during the Ag-catalyzed etching process. Furthermore, the ability to strongly suppress reflection for the porous SiNC arrays in a wide wavelength range of 300-1700nm is demonstrated by simulation calculation and experimental test.

EXPERIMENTAL

Mirror polished n-type Si(100) wafers with a resistivity of 3-5 Ω·cm were used as the starting substrates to fabricate the SiNC arrays. The wafers were cleaned according to previously reported procedures.[23] In brief, this involved the removals of polymer contaminants and native oxide. Ag films of ~ 5 nm thickness were deposited on the cleaned Si substrates by magnetron sputtering, and this produced the interconnected Ag nanoislands.[22] The nanoislands coated substrates were subsequently immersed into etching solution containing H_2O_2 with different concentrations and HF with same concentration of 5 M. After etching, the samples were rinsed in dilute nitric acid to remove the residual Ag.

The morphologies of the porous SiNC arrays were characterized using scanning electron microscopy (SEM) with a FEI Quanta 200F and a high resolution transmission electron microscopy (HRTEM) with a Tecnai G^2 F20. The redox reactions in the Ag-catalyzed etch process were analyzed by electron spin resonance (ESR) with a Bruker ESP 300E. The total reflection spectra of the porous SiNC arrays were measured by a solar cell IPCE/QE measurement system with an integrating sphere.

RESULTS AND DISCUSSIONS

Table I summarizes the studied conditions and the results of the produced SiNC arrays. The successful growth of porous SiNC arrays using the Ag-catalyzed etching method is illustrated by the images of Fig. 1. SiNC arrays with a length of ~ 400 nm are observed, uniformly covering the Si substrate (Fig. 1a). A large majority of the nanocones are very straight. The morphologies of the hooked or ground-collapsed SiNWs obtained by an Au-assisted etching in the HF/H_2O_2 solution with a certain proportion have not been observed.[18] Moreover, a high density of nanopores is observed at the sidewalls of the nanocones (Fig. 1b). A core-shell structure (HRTEM of Fig. 1c) is observed consisting of a single-crystalline core (inset in Fig. 1c) covered in a ~ 6 nm thick layer of an amorphous porous shell.

For Au-catalyzed etching, it has been reported that nanocone formation is attributed to the tapering of nanowires resulting from diffusion of the excess holes along the nanowire axial direction.[20] The tapering level is determined mainly by the amount of the excess holes, which is experimentally dependent on the concentration of H_2O_2 in etchant solution[18,19] and etch duration.[19] To test whether

TABLE I. Lengths and densities of the SiNC arrays obtained under different process parameters.

	Process parameters		Porous SiNC arrays	
Sample	H_2O_2 concentration (M)	Etching time (min)	Length (nm)	Density (mm^{-2})
1	0.05	10	290	6.5×10^7
2	0.2	2	400	7.1×10^7
3	0.5	2	800	6.3×10^7
4	0.5	3	1470	6.6×10^7

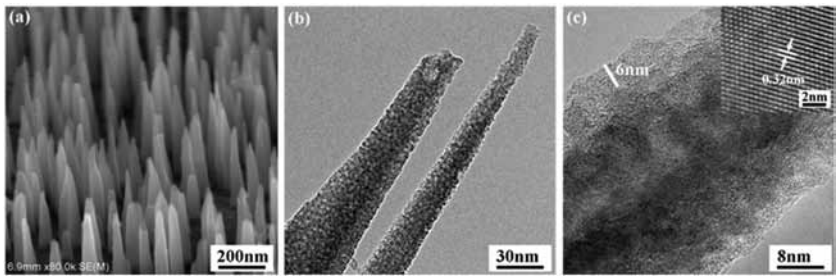

FIG. 1. Morphologies of the porous SiNC arrays obtained by Ag-assisted etching in a solution containing 5 M HF and 0.2 M H_2O_2 for a 2 min duration. (a) SEM image of the porous SiNC arrays. (b) TEM image of the porous nanocones. (c) HRTEM image of individual nanocone. Inset image in (c) is a high-magnified HRTEM image of a selected area of the nanocone.

the nanocone formation for the case of the Ag-catalyzed etching used here also relates to excess hole diffusion, samples were etched under different H_2O_2 concentrations (as summarized in Table I) and their morphologies were observed. We found that for the range of H_2O_2 concentrations studied, SiNC arrays were always obtained, as exemplified by the SEM images for 0.05 M H_2O_2 (Fig. 2a) and 0.5 M H_2O_2 (Fig. 2b) concentrations. For a given H_2O_2 concentration, the length of the nanocone increased with increasing etch time (Fig. 2c). The taping level of these nanocones has been measured by using the protractor software. The angle between nanocones and the Si substrate did not change significantly and were in the range of 85.0°∼87.0°, which suggest that the excess hole diffusion is rarely involved in the growth process.

To understand the nanostructural evolution with etching time, a mechanism for porous SiNC arrays formation is proposed. The mechanism is based on redox reactions at the Ag/Si interface and the Ag/solution interface.

At the Ag/Si interface, the Ag nanoislands act as a conducting electrode for transferring electrons from Si to the H_2O_2 solution (Eq.(1)). The generated SiO_2 (Eq. (2)) underneath the Ag nanoislands is immediately dissolved by the HF solution, making the Ag nanoislands sink into the bulk of the Si wafer. The nanoislands do not drop off in these regions because they are trapped by the forming SiNC surrounding them.

$$H_2O_2 + 2H^+ + 2e \rightarrow 2H_2O \tag{1}$$

$$Si + 2H_2O \rightarrow SiO_2 + 4H^+ + 4e \tag{2}$$

At the Ag/solution interface, Ag nanoislands are gradually dissolved to Ag^+ ions in the presence of H_2O_2, leading to a progressive decrease in the nanoisland size with etching time. However, for the Ag-catalyzed etching, the specific reactions involved between Ag and H_2O_2 are uncertain. Hence, the dissolution reactions and intermediate products during the Ag-catalyzed etching processes (as proposed above) were further studied using electron spin resonance spectroscopy. A few spin trap agents were adopted to detect possible products such as hydroxyl radicals (·OH), superoxide (O_2^{g-}) and singlet oxygen ($^1O_2$).[25–27] Only ·OH were detected when a DMPO spin trap agent was used, as shown by the characteristic peaks in Fig. 3a. The ·OH generation implies that the dissolution of

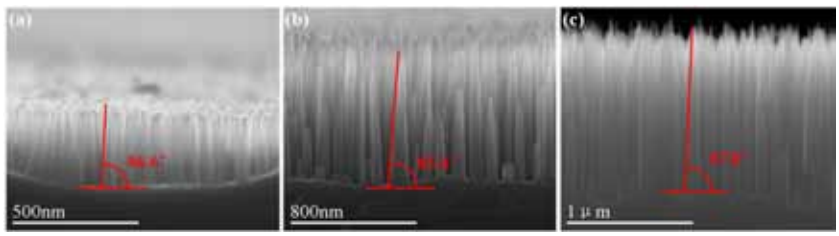

FIG. 2. Cross-sectional morphologies of the porous SiNC arrays obtained with different concentrations of H_2O_2 and reaction time. (a) 0.05 M/10 min; (b) 0.5 M/2 min; (c) 0.5 M/3min.

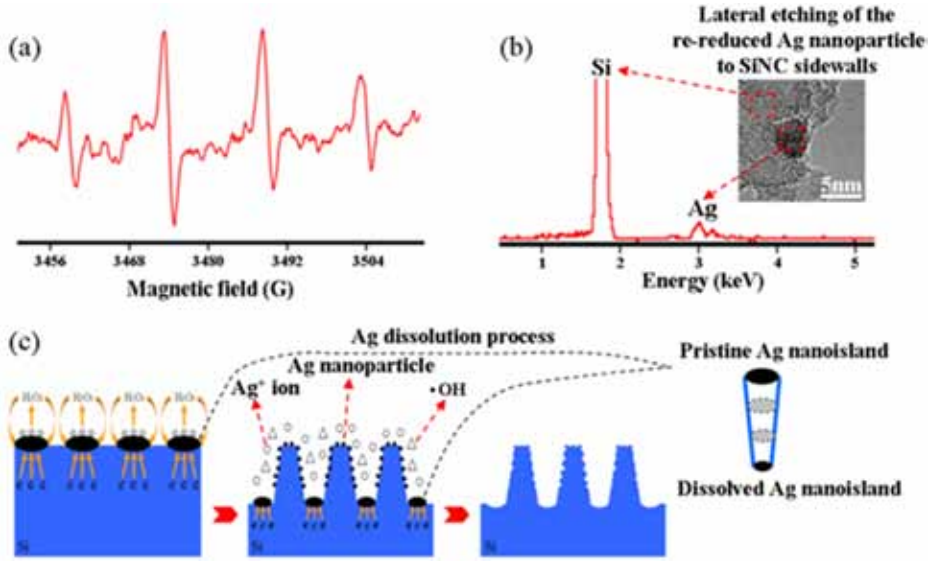

FIG. 3. (a) ESR spectrum of the etching solution added with DMPO spin traps during the etching process; (b) HRTEM image of the Ag NPs-embedded SiNC and the corresponding EDX spectrum; (c) Schematic diagram of the redox processes for Ag nanoisland-catalyzed chemical etching of the Si in HF/H_2O_2 solution.

Ag nanoislands involves a Fenton-like[25] reaction (as described by Eq. (3)).Therefore, for our Ag-catalyzed etching process, the tapered growth of porous SiNC results from continuous dissolution of Ag to Ag^+ ions, resulting in the gradual shrinkage of the Ag nanoislands, which leads to tapering of the SiNC, as shown in Fig. 3c.

$$Ag + H_2O_2 + H^+ \rightarrow Ag^+ + \cdot OH + H_2O \tag{3}$$

$$Ag^+ + e \rightarrow Ag \tag{4}$$

The generated Ag^+ ions nearby the nanopillar sidewalls gets re-reduced to fine Ag nanoparticles(NPs) at SiNC sidewalls according to the reaction (Eq. (4)) because the redox level of the Ag^+/Ag system lies below the valance band of silicon,[28] giving the lateral etching of the re-reduced Ag NPs to SiNC sidewalls (as observed in Fig. 3b) and hence producing the porous SiNC.

According to the effective refraction theory, reflectance spectra of the porous SiNC arrays are simulated through a multilayer model and the transfer matrix formalism method.[1,16,29] Model building of the porous SiNC arrays and the corresponding calculation are described in the supplementary material.

To understand the correlation between surface quality of the nanocone and their reflectance, reflectance spectrum of the SiNC arrays with smooth surface and porous surface are compared. Two types of SiNC arrays keep a same thickness of 1μm and filling ratio of 7.0×10^7 mm^{-2}. From the image of Fig. 4, it can be seen that the reflectance of the porous SiNC arrays is much lower than that of the smooth SiNC arrays in the wavelength range of 300-1700nm. It is well known that the SiNC arrays can remarkably reduce surface reflection loss over a broad range of wavelengths due to a gradual reduction of the effective refractive index between air and silicon.[15,16,22] The above calculated result indicates that introducing nanopore to SiNC surface can further improve the broadband antireflection properties of the SiNC arrays.

To further study the effect of surface quality of the nanocone on their reflectance, reflectance spectra of the porous SiNC arrays with different porosity on nanocone surface are calculated. The porous SiNCs have a same length of 1μm. The effective refraction index varying with the wavelength of light is shown in the supplementary material. For the arrays of porous SiNC with different porosity, the upward trend of the effective refractive index between air and silicon slow down gradually when the porosity of the SiNCs increases (the inset image in Fig. 5). Corresponding, reflectance

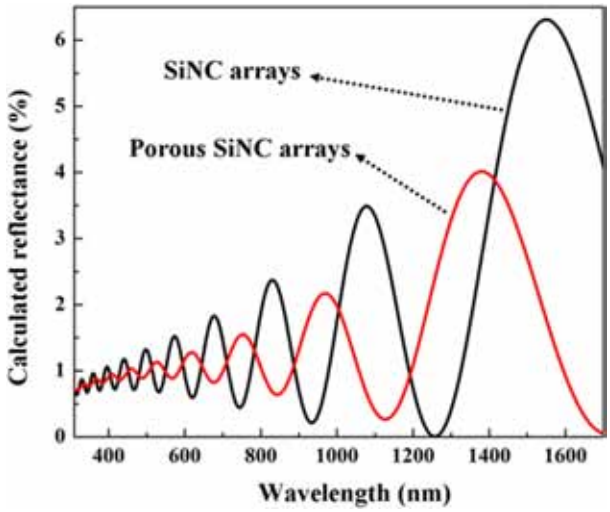

FIG. 4. Comparison of calculated reflectance spectra of the SiNC arrays with smooth surface and porous surface.

of the porous SiNC arrays gradually reduces with increasing their porosity (Fig. 5). It is noted that the reflectance drops significantly in the long-wavelength range of 1400-1700nm, suggesting that increasing porosity of SiNC surface is a potential approach to reduce the long-wavelength reflection loss.

Calculated and experimental reflectance spectra of the porous SiNC arrays with different lengths were studied. Calculated results show that the reflectance spectra of these porous SiNC arrays seem to be composed of various interfering fringes, whose amplitudes gradually reduce with increasing the length of porous SiNC arrays (Fig. 6(a)). When the length of porous SiNC arrays increases to 1500nm, the reflectance spectrum turns to be a straight line and the reflectance value is below 2.2% in the wavelength range of 300-1700nm.

From the experimental data of Fig. 6(b), it can be seen that the porous SiNC arrays with a length of 290 nm reduce the average reflectance from 39.6% (polished Si) to 22.5% in the wavelength range of 300-1000nm. Surface reflection is further suppressed by increasing the length of the porous SiNC arrays. The average reflectance of 1470nm long porous SiNC arrays is about 1.7%,

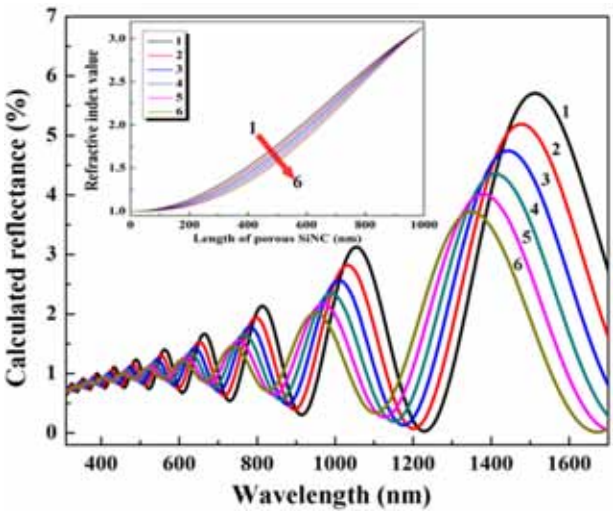

FIG. 5. Calculated reflectance spectra of the porous SiNC arrays with different porosity on nanocone surface; Inset in Fig. 5 shows the relation between surface porosity of the porous SiNCs and their refraction index.

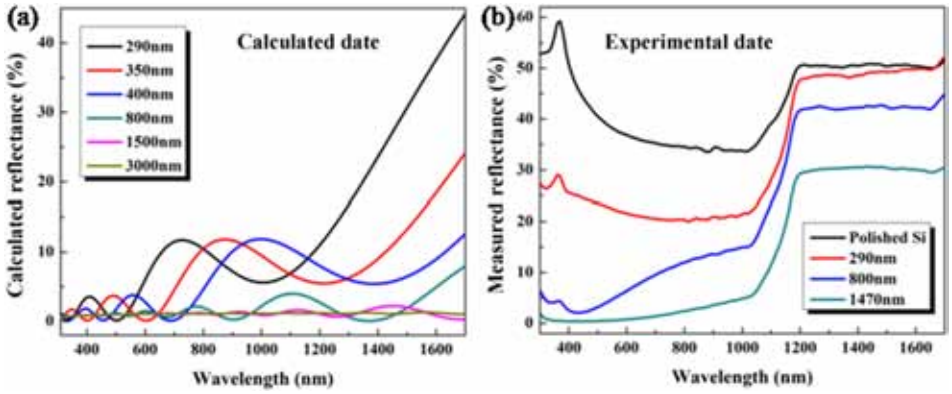

FIG. 6. (a) Calculated and (b) experimental reflectance spectra of the porous SiNC arrays with different lengths.

which is generally consistent with our calculation result and is also approaching the lowest values previously reported for 1.6μm long Si nanotip arrays[15] as well as highly ordered 10μm long SiNW arrays.[30]

Furthermore, the long-wavelength antireflection performance of the porous SiNC arrays is also experimentally verified and shown in Fig. 6(b). The average reflectance in the wavelength range of 1200-1700 nm reduces from 50.5% to 30.1% with increasing length of the porous SiNC arrays, suggesting that increasing length of SiNC surface is another effective way to reduce the long-wavelength reflection loss. Notably that the difference between calculated and experimental reflectance spectra is inevitable. These differences are resulted from the sum of these reasons such as amorphous porous shell of the produced porous SiNCs, their non-uniform length and diameter, their random distribution on Si substrate and so on.

CONCLUSION

We have reported a simple Ag-assisted chemical etching approach for the fabrication of the porous SiNC arrays. In Ag-assisted etching process, the hydroxyl radical is detected and a redox process based on gradual dissolution of the Ag nanoislands and lateral etching of the regenerated Ag nanoparticles is proposed to explain the formation mechanism of the porous SiNC arrays. Moreover, calculation results revealed the broadband antireflection properties of the porous SiNC arrays. Especially in long-wavelength range, the reflectance can be further reduced by increasing surface porosity of the SiNCs and their length. Furthermore, the experimental results generally fit our calculation results. The produced porous SiNC arrays exhibit a low average reflectance of 1.7% in the wavelength range of 300-1000nm and approximately 30% in the wavelength range of 1200-1700nm, which is expected to open new applications in Si-based infrared detectors[31] and long-wavelength absorption devices in photovoltaic/thermal hybrid solar system.[32]

SUPPLEMENTARY MATERIAL

See supplementary material for Reflectance of the porous SiNC arrays is calculated with a multilayer model. A cylindrical coordinate system is used, in which the Z-axis is perpendicular to the substrate surface. The bottom of SiNW is at Z=0 and the peak at Z=h. The SiNW is divided into N horizontal layers with the thickness of each layer denoted dj, where j=1...N. Each layer has the same thickness, d1=dN=d, in our calculations. The radius of the SiNW, R, in each layer satisfies $R^2=(h-z)r^2/h$ and $R=(h-z)r/h$ for $0<z<h$ for the paraboloid and cone structures, respectively. There, each layer has a different filling ratio $f_j=\pi R^2$, resulting in stepwise-varying refraction index profiles. The imaginary part of the refraction index was considered in calculations to match the absorption nature of Si.

ACKNOWLEDGMENTS

This work is supported partially by National High-tech R&D Program of China (863 Program, No. 2015AA034601), National Natural Science Foundation of China (Grant nos. 91333122, 51372082, 51402106 and 11504107),Ph.D. Programs Foundation of Ministry of Education of China (Grant nos. 20130036110012), Par-Eu Scholars Program, Beijing Municipal Science and Technology Project (Z161100002616039) and the Fundamental Research Funds for the Central Universities (2016JQ01,2015ZZD03, 2015ZD07). RH acknowledge support from the ERC (Advanced Investigator Grant, Novox, ERC-2009-adG 247276) and Cambridge Commonwealth Trusts and the Rutherford Foundation of New Zealand.

[1] S. Chattopadhyay, Y. F. Huang, Y. J. Jen, A. Ganguly, K. H. Chen, and L. C. Chen, Mater, Sci. Eng. R. **69**, 1 (2010).
[2] S. S. Walavalkar, C. E. Hofmann, A. P. Homyk, H. A. Atwater, and A. Scherer, Nano Lett. **10**, 4423 (2010).
[3] J. K. Kim, S. Chhajed, M. F. Schubert, E. F. Schubert, J. Cho, H. Kim, and C. Sone, Adv. Mater. **20**, 801 (2008).
[4] X. W. Geng, Z. Qi, M. C. Li, B. K. Duan, and L. J. Zhu, Sol. Energy Mater. Sol. Cells. **103**, 98 (2012).
[5] Y. F. Li, M. C. Li, P. F. Fu, R. K. Li, D. D. Song, C. Shen, and Y. Zhao, Sci. Rep. **5**, 11532 (2015).
[6] Y. F. Li, L. Yue, Y. N. Luo, W. J. Liu, and M. C. Li, Opt. Express. **24**, A1075 (2016).
[7] Y. F. Li, M. C. Li, D. D. Song, H. Liu, B. Jiang, F. Bai, and L. H. Chu, Nano Energy **11**, 756 (2015).
[8] J. Y. Jung, H. D. Um, S. W. Jee, K. T. Park, J. H. Bang, and J. H. Lee, Sol. Energy Mater. Sol. Cells. **112**, 84 (2013).
[9] L. Hu and G. Chen, Nano Lett. **7**, 3249 (2007).
[10] S. K. Srivastava, D. Kumar, P. K. Singh, V. Kumar, and M. Husain, Sol. Energy Materi. Sol. Cells. **94**, 1506 (2010).
[11] L. Tsakalakos, J. Balch, J. Fronheiser, J. Fronheiser, and U. Rapol, J. Nanophotonics. **1**, 013552 (2007).
[12] V. Sivakov, G. Andra, A. Gawlik, J. Plentz, F. Falk, and S. H. Christiansen, Nano Lett. **9**, 1549 (2009).
[13] J. Zhu, Z. F. Yu, G. F. Burkhard, C. M. Hsu, Q. Wang, M. McGehee, S. H. Fan, and Y. Cui, Nano. Lett. **9**, 279 (2009).
[14] J. Y. Jung, Z. Y. Guo, S. W. Jee, H. D. Um, K. T. Park, and J. H. Lee, Opt. Express **18**, A286 (2010).
[15] Y. F. Huang, S. Chattopadhyay, Y. J. Jen, K. H. Chen, and L. C. Chen, Nat. Nanotechnology **2**, 770 (2007).
[16] A. Najar, P. Pirasteh, J. Charrier, and R. Sougrat, Opt. Express **20**, 16861 (2012).
[17] C. Wu, C. H. Crouch, L. Zhao, J. E. Carey, R. Youkin, J. A. Levinson, and E. Mazur, Appl. Phy. Lett. **78**, 1850 (2001).
[18] D. H. Lee, Y. K. Kim, G. S. Doerk, I. Laboriante, and R. Maboudian, J. Mater. Chem. **21**, 10359 (2011).
[19] M. K. Dawood, T. H. Liew, P. Lianto, M. J. T. L. Thong, and W. K. Choi, Nanotechology **21**, 205305 (2010).
[20] B. P. Azeredo, J. Sadhu, J. Ma, K. Jacobs, J. Kim, K. Lee, J. H. Eraker, and K. Hsu, Nanotechology **24**, 225305 (2013).
[21] M. K. Dawood, S. Tpathy, S. B. Dolmanan, T. H. Ng. H. Tan and J. Lam, J. Appl. Phys. **112**, 073509 (2012).
[22] F. Bai, M. C. Li, R. Huang, Y. F. Li, M. Trevor, and K. P. Musselman, RSC Adv. **4**, 1794 (2014).
[23] F. Bai, M. C. Li, D. D. Song, H. Yu, B. Jiang, and Y. F. Li, J. Solid State Chem. **196**, 696 (2012).
[24] F. Bai, M. C. Li, R. Huang, Y. Yu, T. S. Gu, Z. Chen, H. Y. Fan, and B. Jiang, J. Nanopart. Res. **15**, 1915 (2013).
[25] W. W. He, Y. T. Zhou, W. G. Wamer, M. D. Boudreau, and J. J. Yin, Biomaterials **33**, 7547 (2012).
[26] D. He, A. M. Jones, S. Garg, A. N. Pham, and T. D. Waite, J. Phys. Chem. C. **115**, 5461 (2011).
[27] G. L. Wang, X. Y. Zhu, Y. M. Dong, H. J. Jiao, X. M. Wu, and Z. J. Li, Talanta **107**, 146 (2013).
[28] Z. P. Huang, N. Geyer, P. Werner, J. D. Boor, and U. Gosele, Adv. Mater. **23**, 285 (2011).
[29] T. H. Pei, S. Thiyagu, and Z. Pei, App. Phys. Lett. **99**, 153108 (2011).
[30] B. Ozdemir, M. Kulakci, R. Turan, and H. E. Unalan, Nanotechnology **22**, 155606 (2011).
[31] A. Zhang, H. K. Kim, J. Cheng, and Y. H. Lo, Nano Lett. **10**, 2117 (2010).
[32] T. T. Chow, Appl. Energy. **87**, 365 (2010).